Invited Paper

Electro-Luminescent Cooling in the Deep Sub-Bandgap Bias Regime

Parthiban Santhanam

Research Lab of Electronics, Massachusetts Institute of Technology, Cambridge, MA 02139

ABSTRACT

Recent work on electro-luminescent cooling has focused either on diodes at forward bias voltages just below the bandgap energy, where high cooling power density is possible, or voltages below the thermal voltage, where the effect is more tolerant to parasitic non-radiative recombination. Here we consider the possibilities for diodes designed to operate at intermediate voltages. Numerical calculations suggest that design for this regime may enable near- and mid-infrared devices capable of solid-state refrigeration with sufficient power density for some applications.

LONG ABSTRACT

Electro-luminescent cooling, in which electrons and holes absorb heat from the lattice and subsequently release it as incoherent radiation, was only recently observed in infrared light-emitting diodes at very low power density. These results utilized the low-bias regime in which the electrical energy qV is much smaller than the thermal energy $k_{\mathrm{B}}T$. Other investigations into electro-luminescent cooling have focused on much higher bias operation where qV is within a few $k_{\mathrm{B}}T$ of the bandgap energy E_{gap}, but have been hampered by the associated requirement of very high quantum efficiency. We find that redesigning devices for the intermediate deep-sub-bandgap bias regime, where $k_{\mathrm{B}}T < qV < E_{\mathrm{gap}} - 3k_{\mathrm{B}}T$, could enable electro-luminescent cooling with higher power density, lower lattice temperature, and emitting shorter wavelength light. At near-infrared wavelengths, a quantum efficiency of 75% could provide milliwatts of room-temperature cooling power per cm^2, roughly 100 times the highest reported figures at any temperature to date.

1 INTRODUCTION

When electro-luminescent cooling, or equivalently electrical-to-optical power conversion above unity wall-plug efficiency, was theoretically proposed over five decades ago its potential as an applied technology was recognized almost immediately [1, 2]. In the subsequent three decades, studies of the effect were sparse, presumably because the most prominent experimental effort to realize the phenomenon, that of Dousmanis, et. al. [3], had led experimentalists to believe that doing so would require extremely good material quality and extraction methods which were not perceived to be within reach at the time.

After several decades of relative inattention, the theoretical work of Paul Berdahl [4], that of Martin Green and co-authors [5, 6, 7], and that of Mal'shukov and Chao [8], renewed interest in the effect and its application to energy conversion and solid-state refrigeration. These results

Laser Refrigeration of Solids VII, edited by Richard I. Epstein, Denis V. Seletskiy, Mansoor Sheik-Bahae, Proc. of SPIE Vol. 9000, 900007 · © 2014 SPIE
CCC code: 0277-786X/14/$18 · doi: 10.1117/12.2040497

were followed by more detailed computational studies by numerous authors suggesting cooling should be achievable in well-studied semiconductor material systems such as AlGaAs [9, 10, 11, 12] and InGaAsP [13], which in turn led to renewed experimental interest.

Apart from the work of the author and his direct collaborators, two recent experimental efforts have been documented, one at Arizona State University and the other at Aalto University in Finland. In parallel with basic theoretical work on the role of heterostructures [14] and low-dimensional systems [15] in the phenomenon, the group at Arizona State fabricated a microstructure [16, 17] designed to produce a 6°C drop due to electro-luminescent cooling. Although the group's publications indicate that a substantial experimental effort was made to realize cooling, net cooling has not been reported as of yet. In addition to publishing the most comprehensive analyses of both the electron transport [10] and thermal transport [11] in light-emitting diodes (LEDs) with above-unity wall-plug efficiency, the group at Aalto University has mounted a substantial effort to realize net cooling experimentally [18, 19]. The approach taken by Aalto differs from the aforementioned work at Arizona State in its focus on design of devices to optimize electron transport and less focus on micro-fabrication designs intended to optimize light extraction and thermal isolation of the emitter. The ongoing work at Aalto University has not yet produced a published result with net cooling either, and recent focus has shifted from the infrared to visible emitters in the GaN material system due in part to the relevance of this work to improving efficiency in solid-state lighting.

Recent work by the author and his collaborators has successfully observed net electro-luminescent cooling at very low cooling power density [20, 21]. These measurements were performed on diodes operating in a very different regime than that explored by previous studies, theoretical or experimental. This approach utilized existing mid-infrared LEDs, whose performance has long been limited by non-radiative recombination as well as imperfect photon extraction, in a novel operating regime. In this case, the diodes were forward biased by a very small voltage V which was much smaller than the thermal voltage $k_{\mathrm{B}}T/q$. In this low-bias regime, the electrical work required to inject each electron-hole pair into the emitter's active region, qV, decreased as the current was reduced while the optical energy, $\hbar\omega$, emitted by each electron-hole pair undergoing radiative recombination remained fixed. Additionally, since the thermal voltage sets the energy scale for rectification, the radiative recombination process exhibits a linear response to the applied voltage, resulting in a fixed nonzero quantum efficiency. That is to say:

$$\lim_{V\to 0^+} \eta_{EQE}(V) \;=\; \eta^0_{EQE} \tag{1}$$

where $\eta_{EQE}(V)$ is the voltage-dependent External Quantum Efficiency (EQE) and η^0_{EQE} is independent of voltage.

Together these facts implied that arbitrarily high efficiency in excess of unity was achievable at sufficiently low voltage, as is readily apparent from the following rather general expression for wall-plug efficiency η of a light-emitter.

$$\eta \;=\; \frac{\hbar\omega}{qV} \cdot \eta_{EQE}(V) \tag{2}$$

While the observation of this general property of light-emitting diodes, applicable to devices

in most inorganic material systems which are well-modeled by the conventional recombination rate equations, may be of scientific interest, the extremely low optical power density limits its utility to applications in which small signals are sufficient and energy consumption is important at the system-level [22, 23].

In particular the main aim of previous work on electro-luminescent cooling, to build a practical device capable of vibration-free solid-state cooling, remains many orders of magnitude in power density away. Nevertheless, much of this difference may be possible to overcome through the explicit design of light-emitting diodes for lower voltages than are currently designed for [10, 24]. Although the low-bias regime $V \ll k_B T/q$ necessarily constrains the electrically-driven optical power density to below that of equilibrium blackbody radiation, design for higher biases which are still several $k_B T$ below E_{gap} remains largely unexplored. This deep sub-bandgap bias regime, for which

$$\frac{k_B T}{q} \; < \; V \; < \; \frac{E_{gap} - 3k_B T}{q} \qquad , \tag{3}$$

represents a promising pathway toward devices which use electro-luminescence for solid-state cooling.

The remainder of this manuscript is arranged into four sections. In § 2, we will review recent work on design for the low-bias regime and compare this process to design for higher bias, higher power-density operation. In § 3 we will outline a design strategy for the deep sub-bandgap bias regime and follow it to generate a design. In § 4, we will briefly describe additional degrees of freedom for which future experiments could reveal information relevant to the design of electro-luminescent cooling diodes. Finally in § 5 we will summarize this work and provide short commentary on the overall state of the science and technology of electro-luminescent cooling.

2 DESIGN FOR LOW BIAS

Recent work by Dodd Joseph Gray, Jr., Rajeev J. Ram, and the author of this manuscript has made use of an experimentally-verified electron transport model to design an InGaAsSb LED for low-bias operation [24]. The design process in this regime is dominated by the need to enhance the device's low-bias quantum efficiency η^0_{EQE}, because this quantity directly determines both the low-power efficiency and the maximum optical power density available at unity efficiency. The constraint on power follows from the constraint on voltage found by evaluating Equation (2) at η=1.

$$V_{max} = \frac{\hbar\omega}{q} \cdot \eta^0_{EQE} \qquad \text{when} \qquad \eta^0_{EQE} < \frac{k_B T}{\hbar\omega} \tag{4}$$

When η^0_{EQE} exceeds this constraint, the maximum voltage bias compatible with unity efficiency is no longer confined to the low bias regime. However, this constraint proved difficult to overcome so the InGaAsSb design problem was reduced to maximizing η^0_{EQE}.

The two primary degrees of freedom which were optimized over in the aforementioned study were the active region doping and its thickness. In both cases, the parameter being optimized over exhibited a unique optimum. The physics behind these design trade-offs are described in Figure 1a and Figure 1b in the cases of active region doping and thickness respectively.

Typically the density of crystal defects and their associated trap states leads to so much non-radiative recombination that mid-infrared LEDs in the GaSb-lattice-matched InGaAsSb material system have very low quantum efficiency. However by introducing dopants into the active region [10], the minority carrier concentration at low bias can be reduced as a consequence of the Law of Mass Action, and the relative importance of the associated Shockley-Read-Hall (SRH) trap-assisted non-radiative recombination can be reduced. Very high dopant concentrations, however, lead to too much non-radiative Auger recombination. As a result, an intermediate optimal doping concentration was found; its value was well-approximated by the analytical form first proposed by Heikkila, in which the acceptor concentration was given by the inverse of the geometric mean of the SRH lifetime (units of s) and the Auger coefficient (units of $\mathrm{cm}^6\mathrm{s}^{-1}$). The optimal acceptor concentration found numerically was 2×10^{16} cm^{-3}.

The thickness of the active layer also plays a role in an LED's η^0_{EQE} due to the reabsorption of photons degrading the photon extraction efficiency. However for a very thin active layer, parasitic recombination processes outside the active region lead to leakage current and decrease the internal quantum efficiency. As a result, an optimal thickness was found to be 1.5 μm.

With the resulting design, under the assumption of a high-quality organometallic vapor phase epitaxy growth that allows for an SRH lifetime of 1 μs [25], it was predicted that a redesigned emitter packaged identically to the experimentally characterized device would have wall-plug efficiency several hundred times greater for the microwatts-per-cm^2 intensities indicative of forward bias on the order of 10 mV. Nevertheless, the net result of optimizing over the thickness and doping of the active region did not increase the low-bias external quantum efficiency enough to allow above-unity efficiency operation for bias voltages above $k_{\mathrm{B}}T/q$.

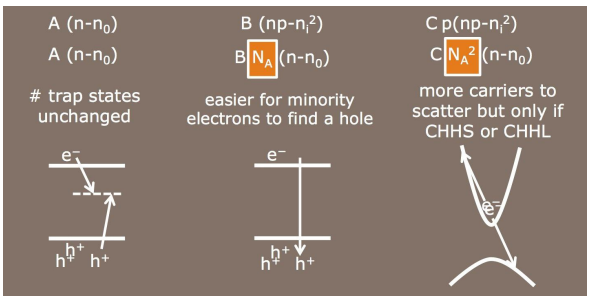

(a) Optimization of active-region doping.

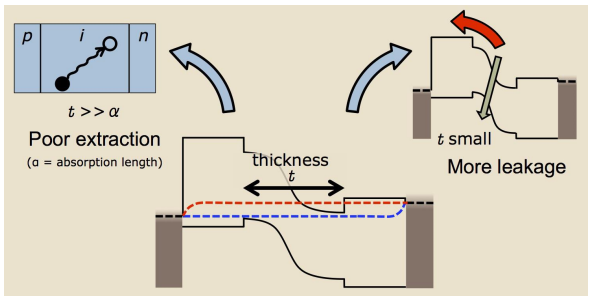

(b) Optimization of active layer thickness.

Figure 1: Depictions of the trade-offs in the two main variables optimized over in the recently reported LED design for low-bias [24]. In (a) the three main recombination processes in the device are depicted (SRH, Bimolecular, and Auger), along with the expressions for their rates per unit volume. The top row of expressions are general; the next row of expressions apply in the case of p-doping. This second row shows the dependence of each rate on the acceptor concentration N_A. In (b), the competing loss mechanisms relevant to active layer thickness optimization are shown. Thick active regions suffer from photon reabsorption while thin active regions enhance the importance of leakage.

3 DESIGN FOR DEEP SUB-BANDGAP BIAS

The device design space considered in the previous section was constrained to a particular material system as the objective was to optimize an LED emitting at a fixed wavelength. In that case, we considered only double hetero-junction diodes whose quasi-neutral regions were composed of pure GaSb and whose active regions were composed of $In_{.15}Ga_{.85}As_{.13}Sb_{.87}$ so that emission would be centered around a free-space wavelength of 2.2 μm. In this section we will free ourselves from this constraint in an attempt to maximize the electro-luminescent cooling power available in the deep-sub-bandgap bias regime regardless of emission wavelength.

We will begin by considering $In_{.15}Ga_{.85}As_{.13}Sb_{.87}$ (lattice-matched to GaSb), $In_{.53}Ga_{.47}As$ (lattice-matched to InP), and pure GaAs. From calculations made based on the recombination rate equations in the previous section, utilizing primarily data aggregated on the NSM Ioffe website [26], we compare the best quantum efficiency achievable in the three material systems at optimal doping. In the case of perfect injection efficiency (i.e. no leakage) and perfect photon extraction (i.e. no internal photon reabsorption or external parasitic loss), we arrive at the results in Table 1.

Material System	A (SRH Recombination)	B (Bimolecular)	C (Auger)	Low-Bias IQE at Optimal Doping
$In_{.15}Ga_{.85}As_{.13}Sb_{.87}$	10^6 s^{-1}	3×10^{-11} cm^{3}s^{-1}	2×10^{-28} cm^{6}s^{-1}	51%
$In_{.53}Ga_{.47}As$	10^5 s^{-1}	10^{-10} cm^{3}s^{-1}	10^{-28} cm^{6}s^{-1}	94%
GaAs	10^6 s^{-1}	7×10^{-10} cm^{3}s^{-1}	7×10^{-30} cm^{6}s^{-1}	99.2%

Table 1: Comparison of three direct-gap III-V materials frequently used in infrared light emitting diodes.

From the right-most column of Table 1 we can infer that η^0_{EQE} varies significantly between the material systems (assuming the efficiency of electron injection and photon extraction are comparable in all three cases). Although Equation (4) does not strictly apply when η^0_{EQE} is greater than $k_{\mathrm{B}}T/\hbar\omega$, for double-hetero-junction LEDs with extrinsic active regions, the domain in which this expression applies can be quite large. From the second row of expressions for the recombination rates shown in Figure 1a, we see that the radiative and non-radiative recombination rates lead to a quantum efficiency independent of bias. Since this expression applies whenever the extrinsic behavior of the active region is visible (i.e. whenever a clear minority carrier species is present), the external quantum efficiency $\eta_{\mathrm{EQE}}(V)$ remains fixed at η^0_{EQE} until

that condition is broken.

$$\eta_{\mathrm{EQE}}(V) = \eta^0_{\mathrm{EQE}} \qquad \text{when} \qquad n_i^2\, e^{qV/k_{\mathrm{B}}T} \;<\; (N_D - N_A)^2 \tag{5}$$

Since the values in the right-most column of Table 1 assume optimal doping, which by definition is chosen to maximize the voltage at which cooling is possible, we may approximate the maximum forward bias voltage at optimal doping using Equation (4) as well.

$$V_{\mathrm{max}} \;\approx\; \frac{\hbar\omega}{q} \cdot \eta^0_{\mathrm{EQE}} \qquad \text{at optimal doping.} \tag{6}$$

From the results in Table 1, it should therefore be clear that the InGaAsSb material is inferior to the InGaAs and GaAs materials in an important way. The total power one could hope to achieve using the InGaAsSb alloy under consideration would be limited by its internal quantum efficiency. Optimally doping the material improves the quantum efficiency at low bias but the maximum voltage allowed for cooling remains constrained by material properties, some of which are addressable like crystal defect densities but others of which are not easily addressed like the rate of Auger recombination.

Material System	Low-Bias EQE with perfect photon extraction (0%, 0%)	Low-Bias EQE with 33% reabsorption, 25% parasitic loss (33%, 25%)	Maximum High-Bias Cooling Power Density (0%, 0%)	Maximum High-Bias Cooling Power Density (33%, 25%)
$In_{.15}Ga_{.85}As_{.13}Sb_{.87}$ $N_D = 7\times10^{16}\mathrm{cm}^{-3}$	51%	31%	5.8 W/m^2	0.11 W/m^2
$In_{.53}Ga_{.47}As$ $N_D = 2\times10^{16}\mathrm{cm}^{-3}$	94%	68%	6.3×10^3 W/m^2	75 W/m^2
GaAs $N_D = 4\times10^{17}\mathrm{cm}^{-3}$	99.2%	74.2%	3.2×10^6 W/m^2	4.5 W/m^2

Table 2: Comparison of theoretical material-based performance limits in the case of both significant (33%) probability for reabsorption in the active region and significant (25%) probability for parasitic absorption after escaping the active region but before escaping the rest of the device. Photon recycling is included as appropriate.

The results of a more complete calculation appear in Table 2. For these calculations we do not make the assumption in Equation (5) but instead directly calculate all recombination rates at all voltages for an active layer of thickness 1 μm. Under the assumption of perfect photon extraction, we find that the wider band-gap materials produce more cooling power. However,

when we include some significant amount of photon absorption, here 33% of generated photons are taken to be reabsorbed within the active layer and 25% of those which escape the active layer are taken to be absorbed in parasitic processes elsewhere in the emitting structure, we find that the intermediate bandgap semiconductor, $In_{.53}Ga_{.47}As$, performs the best. In essence, this is because once the bandgap becomes wide enough for Auger processes not to dominate at the high-voltage end of the deep-sub-bandgap bias regime, parasitics which directly affect the quantum efficiency (i.e. not via the carrier concentration-dependent recombination rates) begin to take a toll proportional to the bandgap. In our case, the 25% parasitic absorption rate plays this role.

As a result of including SRH recombination, Auger recombination, and crude models of photon extraction, we therefore arrive at the result shown in the right-most column of Table 2: the intermediate bandgap semiconductor $In_{.53}Ga_{.47}As$ is the most promising candidate. From here, therefore, we will proceed to design a double-hetero-junction LED for electro-luminescent cooling in the InGaAs/InP material system.

The steps we will follow in the design process are:

1. Determine the dopant type based on Auger rates and/or hetero-junction band alignments.
2. Choose the dopant concentration to maximize the low-bias Internal Quantum Efficiency (IQE), denoted here η^0_{IQE}.
3. Optimize the thickness of the active layer to maximize cooling power.

Step 1. Here we must decide whether to n-type dope or p-type dope the active region. In the previous InGaAsSb design, the performance of p-type doped active regions was far superior to that of the n-type doped active regions due to the importance of bulk SRH recombination in the vicinity of the hetero-interfaces. This issue can be entirely avoided, however, by placing the junction between n-type material and p-type material away from any such interfaces. Here we accomplish this by having a small fraction of the active region be of one polarity while the remainder is of the opposite polarity; this contrasts with the design space considered in the InGaAsSb study where the entire active region was constrained to having a constant dopant concentration and polarity.

Once the importance of band alignments at hetero-interfaces has been reduced by this strategy, the relative magnitude of the various Auger recombination processes in lattice-matched InGaAs can serve as the primary consideration for our design. Despite the maturity of the InGaAs material system, there remains some degree of disagreement in the literature as to the relative magnitudes of the CCCH, CHHS, and phonon-assisted Auger processes [27]. Work by Takeshima suggests phonon-assisted processes should dominate [28], while work by Dutta and Nelson suggests the CHHS process should be dominant over the CCCH process [29]. In either case, however, no results indicate that CCCH processes should be the sole dominant process, so we choose here to n-type dope the active region to suppress CHHS processes at the expense of increased CCCH Auger recombination.

Step 2. We perform this step computationally using the parameters from Table 1 above. The

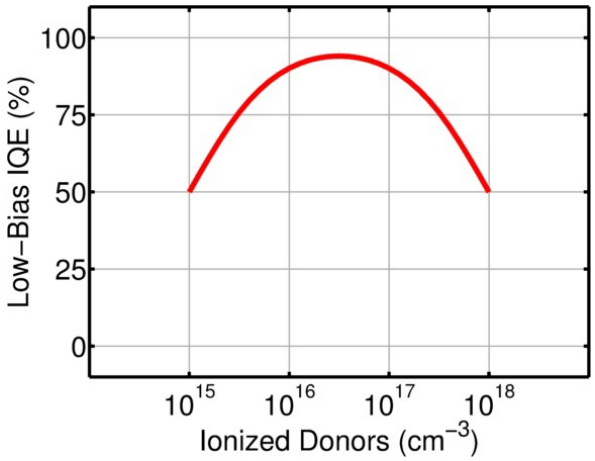

(a) Low-bias IQE vs n-type doping.

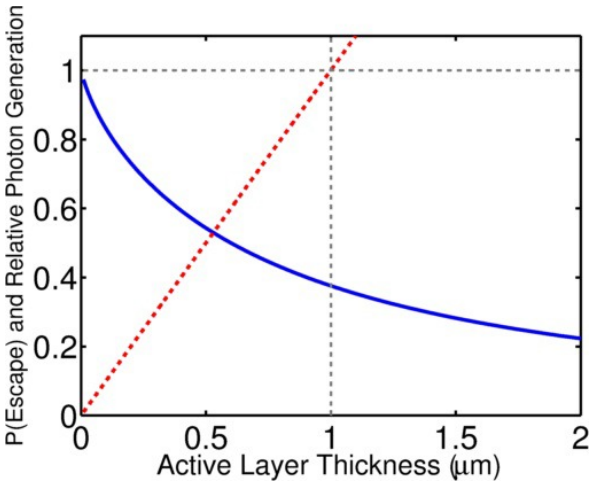

(b) Probability of photon escape (solid blue) and relative photon generation rate (dashed red) vs active layer thickness.

Figure 2: The maximum power density and efficiency that an electro-luminescent cooling LED can generate depends on both the doping and thickness of the active region in which the entropy-carrying photons are generated. The plots above represent results in the InGaAs material system.

results appear in Figure 2a. The optimal doping, defined by maximizing η^0_{IQE}, is n-type doping with a concentration of approximately $2{\times}10^{16}$ cm^{-3}.

Step 3. We begin our final step by considering the layer stack in Table 3, chosen based on previous steps and conventional LED design principles, and vary the active layer thickness to find the optimal layer stack shown in Table 4. For this step we perform electron transport simulations using the commercial software package SimWindows [30] and find the probability of active region reabsorption using our own numerical calculations.

In the previous InGaAsSb design we found that leakage currents were significant enough to justify not using a thin active layer, but they are not sufficient to constrain the design in this case. Instead we find a unique optimal layer thickness which is primarily determined by the trade-off between increased photon reabsorption in a thick layer and reduced power from small total active volume in a thin layer.

First we will discuss our stack in Table 3. The active region is comprised mostly of an n-type InGaAs layer with N_D = 3e16 cm^{-3}. We have increased the donor concentration from the previous step because our SimWindows simulation includes SRH recombination at the p-n homo-junction, which serves to move the optimal doping level up slightly compared with our previous calculation in which we had assumed a spatially homogeneous unipolar active region. We also include a small p-type region (N_A = 3e16 cm^{-3}) at the anode end of the narrow-gap active region in order to move the p-n junction location, where SRH recombination is greatest,

400 nm	of InP	with $N_D = 3e16$ cm^{-3}
900 nm	of InGaAs	with $N_D = 3e16$ cm^{-3}
95 nm	of InGaAs	with $N_A = 3e16$ cm^{-3}
5 nm	of InGaAs	with $N_D = 2e18$ cm^{-3}
5 nm	of InP	with $N_A = 2e18$ cm^{-3}
345 nm	of InP	with $N_A = 1e18$ cm^{-3}
50 nm	of InP	with $N_A = 2e18$ cm^{-3}

Table 3: The suboptimal layer stack prior to optimization of the active layer thickness. Here the thickness of the lattice-matched InGaAs active region is 1 μm.

away from all hetero-junctions.

The 1 μm-wide InGaAs layer is sandwiched between a pair of 400-nm thick n- and p-type InP layers, which are in turn sandwiched between metal contacts taken to be ohmic to form a single p-n double hetero-junction LED. We omit further discussion of the choice of quasi-neutral layers here, in part because their choice is conventional and leakage current was found to be minimal even with a simple design. Additionally, a pair of heavily doped layers of opposite sign were introduced at the p-side hetero-junction to minimize the detrimental effects of voltage drop on the InP side due to low hole mobility and high Auger rates on the InGaAs side due to high hole concentrations.

SimWindows models of the layer stack in Table 3 and the associated family of layer stacks with variable active region thickness were used to calculate the total rate of electron-hole recombination as a function of position. For the non-radiative pathways, these processes were integrated over all positions between the contacts to account for all current due to non-radiative recombination. To good approximation the bimolecular radiative recombination rate was of constant magnitude across the InGaAs active region and of negligible magnitude in the quasi-neutral InP regions for all bias points in the deep-sub-bandgap bias regime. This observation allowed us to perform part of the optimization process without extensive computation by taking the total rate of photon generation to be roughly linearly proportional to the active layer thickness. In more complete SimWindows simulations, we found that very wide active regions led to such high currents that the voltage drop across the quasi-neutral regions was no longer negligible. As a result, the total photon generation rate drooped below the linear approximation at large thickness and thus moved the optimal thickness down slightly.

We estimated the optimal thickness under the assumption that the photon generation rate was linearly proportional to thickness using the 1 μm point for reference. The probability for a given photon to escape as a function of layer thickness was derived analytically in previous work [31, 24]; this result was used along with the internal quantum efficiency from the SimWindows recombination rates for a 1 μm-wide InGaAs layer to compute the extraction efficiency for photons. Since leakage currents were minimal even at 1 μm and the optimal thickness was wider than this point, we were able to assume the IQE was independent of thickness before

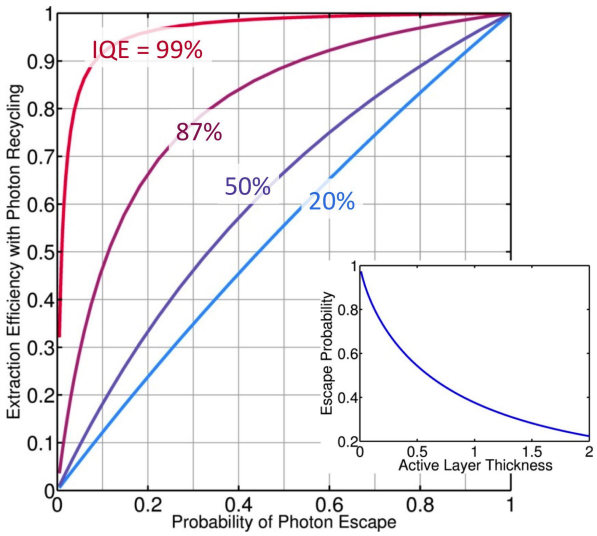

(a) Main figure: Extraction efficiency versus probability for a newly generated photon to escape for various values of the Internal Quantum Efficiency (IQE). Inset: Probability for a newly generated photon to escape versus thickness of the active region.

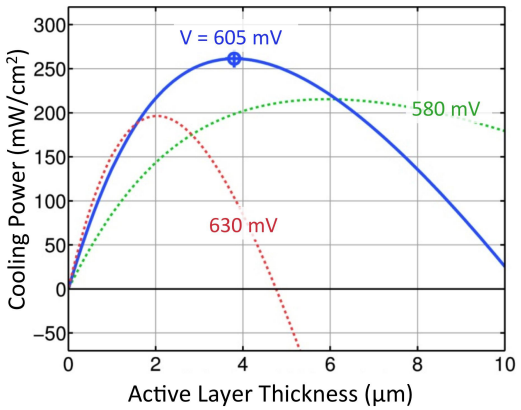

(b) Cooling power density versus active layer thickness at three different bias voltages under the assumption that the photon generation rate is linearly proportional to thickness. The optimal bias and thickness are indicated by the circled cross at the peak of the solid blue curve.

Figure 3: LEDs made with materials of higher IQE benefit more from photon recycling and can remain efficient even when the active layer is relatively thick. For InGaAs, the optimal thickness we find under the assumption that the total photon generation rate is linearly proportional to active region thickness is 3.8 μm.

active region reabsorption was taken into account. For clarity, we remind the reader that the extraction efficiency refers to the ratio of emitted photons to generated photons. In contrast, the product of the photon escape probability P_{escape} and the photon generation rate neglects the possibility of reabsorbed photons contributing to further radiative recombination, an effect known as photon recycling. As is clear from Figure 3a, this photon recycling effect is extremely important in the case of high internal quantum efficiency as in InGaAs under deep-sub-bandgap bias.

In order to choose an optimal design, we needed to calculate the electro-luminescent cooling power density from these device models. We calculated the cooling power density P_{cool} from the recombination rates as

$$P_{\text{cool}} = \hbar\omega \cdot J_{\text{photon}} - \left(J_{\text{photon}} + \int_0^L R_{\text{non-rad}}(z)\, dz \right) qV \tag{7}$$

where $\hbar\omega$ is the photon energy (taken here as the average photon energy emitted from a 3-dimensional semiconductor with parabolic joint density-of-states, $E_{\text{gap}} + k_{\text{B}}T \cdot \Gamma(\frac{5}{2})$), 0 and L are the positions of the cathode and anode contacts respectively, and $R_{\text{non-rad}}$ is the sum of the Auger and SRH recombination rates per unit volume as calculated in the SimWindows model. The symbol J_{photon} refers to the number flux density of emitted photons, which we calculate as follows.

$$J_{\text{photon}} = R_{\text{rad}} \cdot t \cdot \frac{P_{\text{escape}}(t)}{1 - (1 - P_{\text{escape}}(t)) \cdot \eta_{\text{IQE}}} \tag{8}$$

Here R_{rad} is the radiative recombination rate in the active region and t is the thickness of the active layer.

By evaluating the above expressions for various values of t, making use of the linear photon generation rate approximation, we arrive at the results in Figure 3b. The space of thicknesses from 100 nm to 10 μm was investigated and the approximate optimal thickness was found to be 3.8 μm.

400 nm	of InP	with N_D = 3e16 cm^{-3}
2900 nm	of InGaAs	with N_D = 3e16 cm^{-3}
95 nm	of InGaAs	with N_A = 3e16 cm^{-3}
5 nm	of InGaAs	with N_D = 2e18 cm^{-3}
5 nm	of InP	with N_A = 2e18 cm^{-3}
345 nm	of InP	with N_A = 1e18 cm^{-3}
50 nm	of InP	with N_A = 2e18 cm^{-3}

Table 4: The optimized layer stack.

Next we used SimWindows to perform more accurate calculations for thicknesses in the vicinity of 3.8 μm. It was found that the optimal thickness was 3.0 μm, slightly thinner than the linear model result as expected; this corresponds to the final layer stack design shown in

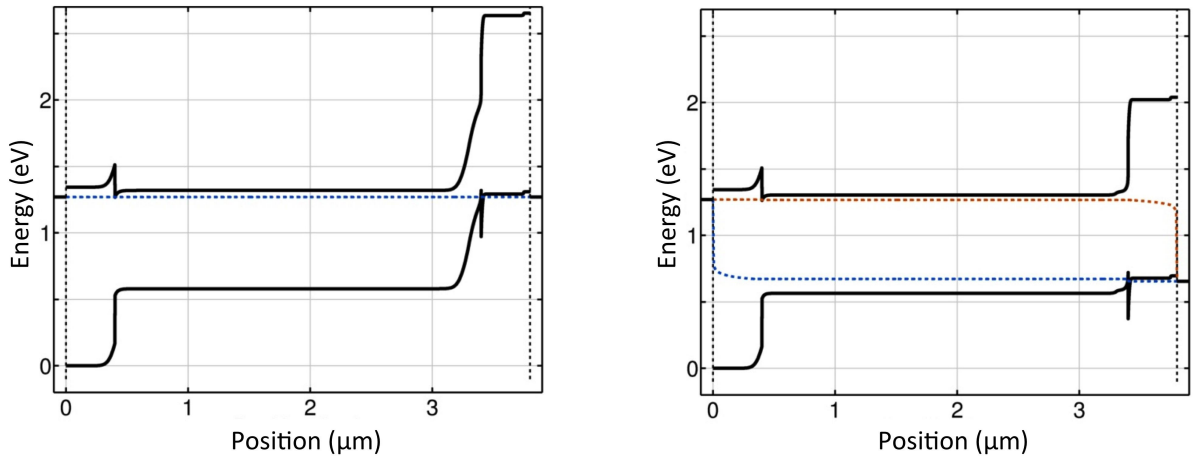

Figure 4: Band diagram of the optimized structure in Table 4 at zero bias (left) and 614 mV forward bias (right). The forward bias point corresponds to the point of maximum electro-luminescent cooling power density.

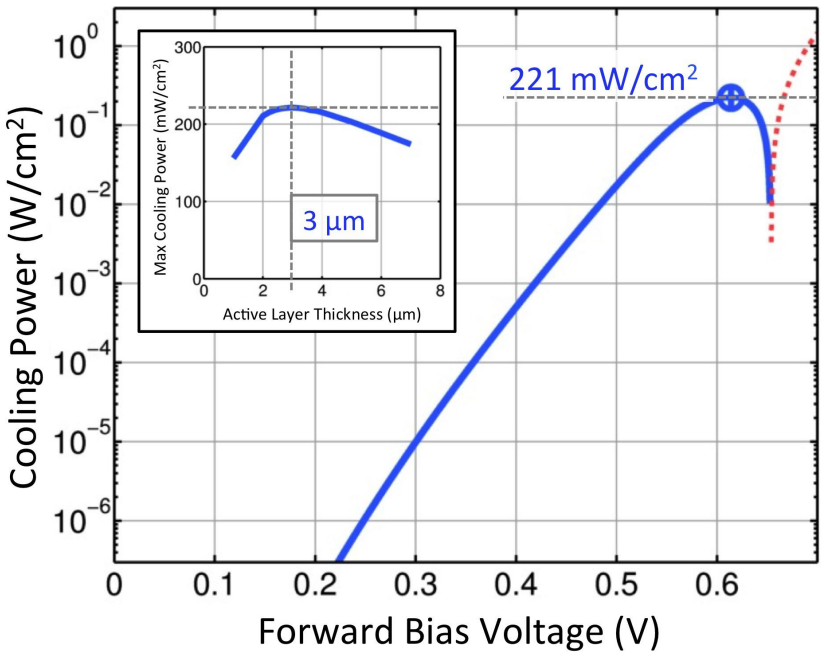

Figure 5: (Main) Electro-luminescent cooling power density versus voltage for the optimized structure whose layer stack appears in Table 4. The solid blue curve is positive cooling power; the dashed red line is negative cooling (i.e. heating). (Inset) Maximum available cooling power for a given device versus active region thickness. A device with active region thickness 3 μm can achieve over 200 mW/cm^2 of electro-luminescent cooling power.

Table 4. Figure 4 depicts the self-consistently solved band diagrams for this final structure at zero bias and the point of maximal cooling power. In Figure 5, we plot the electro-luminescent cooling power density for our optimized device which we find to be just over 220 mW/cm^2 at 614 mV of forward bias voltage. We note that this is 126 mV below E_{gap}/q and falls within the deep-sub-bandgap bias regime as defined in Equation (3).

We conclude this section by highlighting an approximation made in this work which could impact the generality of our device design strategy. Throughout this analysis we assumed that the spectrum of emitted photons was independent of bias voltage. While this is true for bias voltages well below the bandgap, the asymmetry between the electron and hole effective masses should cause the spectrum to blue-shift slightly due to band-filling when the Fermi-level separation ($\approx qV$) exceeds $E_{\text{gap}} - k_{\text{B}}T\ln(N_V/N_C)$, where N_V and N_C denote the effective density of states at the valence and conduction band edges respectively. This should in principle occur only above 647 mV in our InGaAs system, but its effect would be more pronounced in a higher-IQE system such as GaAs. As we outlined previously though, the space of operating points which demonstrate net cooling are unlikely to overlap with this region in any real experiment, since some non-trivial amount of parasitic absorption is to be expected.

4 FUTURE DIRECTIONS

The model of electron transport used in the preceding analysis made several assumptions which simplified the calculation of recombination rates. In the case of SRH recombination, we assumed that all traps lie at the intrinsic Fermi level. For Auger recombination, as we explained previously, we assumed the majority-electron type and majority-hole type Auger processes contribute equally. In any real material system, both of these assumptions are sure to be approximate at best, and at worst may lead device behavior to differ significantly from our calculated results.

In future work, replacing these assumptions with more sophisticated models could yield new designs with superior performance. For example, if majority-electron type CCCH Auger processes are found to be slower, more heavily n-type doping could lead to looser dependence of the low-bias IQE on Auger, moving the optimal doping concentration up. Devices with more n-type doping could therefore perform better in terms of maximum power density as well.

If the SRH lifetime of the two carrier species are found to be significantly different, the sign of the doping could substantially change the total rate of SRH recombination, especially at lower bias voltages where high-efficiency refrigeration is possible. For example, if the trap-assisted hole lifetime τ_{p} is much shorter than that of its electrons τ_{n}, electing to p-dope the active region material would result in a small minority electron population, and further constrain the SRH pathway's bottleneck electron capture step.

Other promising strategies going forward include the use of near-field and Purcell effects to enhance cooling power, the cascading of multiple diodes as is done routinely with thermo-electric coolers [32], and optical extraction designs which employ surface plasmon resonances [33].

5 SUMMARY AND CONCLUSIONS

In this work we have designed a layer stack for a double hetero-junction LED capable of delivering approximately 200 mW/cm^2 of electro-luminescent cooling power at sub-bandgap forward bias voltages. We found that designs with an InGaAs active layer surrounded by lattice-matched InP quasi-neutral layers were superior to designs in the InGaAsSb/GaSb material system due to Auger processes and more robust to parasitics than designs in the AlGaAs material system. By varying the active layer thickness as well as the type and density of doping in this layer, we generated a layer stack optimized for efficient deep-sub-bandgap operation.

The power density of such a design is still substantially below that of competing solid-state cooling technologies like thermo-electric coolers and anti-stokes laser cooling of rare-earth doped glasses. Nevertheless, a working realization of such a device could enable certain new technological capabilities. For example, because radiation is the only heat sink available to spacecraft and the efficiency of laser cooling is bounded by the fluorescence linewidth [34], electro-luminescent cooling could allow spacecraft to actively cool themselves for the benefit of heat-generating onboard electronics. Other examples include low-power digital communication in which the efficiency of the optical source is critical [23] or remote sensing applications [22, 35]; in these applications efficiency is more important than power so long as the source can exceed the very loose constraint of the photo-detector's noise equivalent power.

In order to go beyond these applications, the power density constraints of emitting into free space will likely have to be addressed. By engineering the photonic density of states in and around the emitter, in particular by introducing absorptive matter within distances much shorter than the emission wavelength, the power density of radiative heat transfer can far exceed the conventional form of Planck's Law [36, 37] to which the designs addressed in this work are still constrained. Exploitation of such near-field heat transfer techniques combined with improvements in materials growth should allow the next generation of LEDs designed specifically for electro-luminescent cooling to approach the power density scale of competing solid state refrigeration technologies.

References

[1] J. Tauc. The share of thermal energy taken from the surroundings in the electro-luminescent energy radiated from a *p-n* junction. *Czechoslovakian Journal of Physics*, 7:275–276, October 1957.

[2] M. A. Weinstein. Thermodynamic limitation on the conversion of heat into light. *Journal of the Optical Society of America*, 50(6):597–602, June 1960.

[3] G. C. Dousmanis, C. W. Mueller, H. Nelson, and K. G. Petzinger. Evidence of refrigerating action by means of photon emission in semiconductor diodes. *Physical Review*, 133(1A):A316–A318, January 1964.

[4] P. Berdahl. Radiant refrigeration by semiconductor diodes. *Journal of Applied Physics*, 58(3):1369–1374, August 1985.

[5] M. A. Green. Third generation photovoltaics: Advanced structures capable of high efficiency at low cost. *Proc. of 16th European Photovoltaic Solar Energy Conference*, page 51, May 2000.

[6] N.-P. Harder, D. H. Neuhaus, P. Wrfel, A. G. Aberle, and M. A. Green. Thermophotonics and its application to solar thermophotovoltaics. *Proc. of 17th European Photovoltaic Solar Energy Conference*, pages 102–106, October 2001.

[7] N.-P. Harder and M. A. Green. Thermophotonics. *Semiconductor Sci. Technol.*, 18:S270–S278, April 2003.

[8] A. G. Mal'shukov and K. A. Chao. Opto-thermionic refrigeration in semiconductor heterostructures. *Physical Review Letters*, 86:5570–5573, June 2001.

[9] J.-B. Wang, D. Ding, S.-Q. Yu, S. R. Johnson, and Y.-H. Zhang. Electroluminescence cooling in semiconductors. *2005 Conference on Lasers and Electro-Optics/Quantum Electronics and Laser Science (CLEO/QELS) Conference*, page QThI7, 2005.

[10] O. Heikkilä, J. Oksanen, and J. Tulkki. Ultimate limit and temperature dependency of light-emitting diode efficiency. *Journal of Applied Physics*, 105:093119–1–093119–9, May 2009.

[11] O. Heikkilä, J. Oksanen, and J. Tulkki. The challenge of unity wall plug efficiency: the effects of internal heating on the efficiency of light emitting diodes. *Journal of Applied Physics*, 107(033105):1–6, February 2010.

[12] S.-T. Yen and K.-C. Lee. Analysis of heterostructures for electroluminescent refrigeration and light emitting without heat generation. *Journal of Applied Physics*, 107(054513):1–4, March 2010.

[13] P. Han, K.-J. Jin, Y.-L. Zhou, H.-B. Lu, and G.-Z. Yang. Numerical designing of semiconductor structure for optothermionic refrigeration. *Journal of Applied Physics*, 101(014506):1–4, January 2007.

[14] S.-Q. Yu, J.-B. Wang, D. Ding, S. R. Johnson, D. Vasileska, and Y.-H. Zhang. Fundamental mechanisms of electroluminescence refrigeration in heterostructure light emitting diodes. *Proc. of SPIE*, 6486(648604):1–6, January 2007.

[15] S.-Q. Yu, J.-B. Wang, D. Ding, S. R. Johnson, D. Vasileska, and Y.-H. Zhang. Impact of electronic density of states on electroluminescence refrigeration. *Solid-State Electronics*, 51:1387–1390, August 2007.

[16] S.-Q. Yu, D. Ding, J.-B. Wang, S. R. Johnson, and Y.-H. Zhang. Electroluminescence refrigeration in semiconductors. *2006 Conference on Lasers and Electro-Optics/Quantum Electronics and Laser Science (CLEO/QELS) Conference*, page JTuD102, 2005.

[17] S.-Q. Yu, N. Rider, D. Ding, J.-B. Wang, S. R. Johnson, and Y.-H. Zhang. Light emitting diodes with extremely high extraction-efficiency for electroluminescence refrigeration. *2007 Conference on Lasers and Electro-Optics/Quantum Electronics and Laser Science (CLEO/QELS) Conference*, page JWA57, 2005.

[18] A. Olsson. Fabrication and characterization of thermophotonic devices. Master of science in technology, Aalto University, Department of Biomedical Engineering and Computational Science, 2011.

[19] J. Oksanen, J. Tulkki, H. Lipsanen, A. Aierken, and A. Olsson. Thermophotonic cooling: Effects of photon transport, emission saturation and reflection losses on thermophotonic cooling & status of the experimental work. Presented at SPIE Photonics West Conference, San Francisco, USA., January 2011.

[20] P. Santhanam, D. J. Gray Jr., and R. J. Ram. Thermoelectrically pumped light-emitting diodes operating above unity efficiency. *Physical Review Letters*, 108(097403), February 2012.

[21] P. Santhanam, D. Huang, R. J. Ram, M. A. Remennyi, and Boris A. Matveev. Room temperature thermo-electric pumping in mid-infrared light-emitting diodes. *Applied Physics Letters*, 103(183513):183513–1–183513–5, November 2013.

[22] P. Santhanam and R. J. Ram. Light-emitting diodes operating above unity efficiency for infrared absorption spectroscopy. *Proc. of the 2012 International Photonics Conference*, page TBA, September 2012.

[23] D. Huang, P. Santhanam, and R. J. Ram. Low-power communication with a photonic heat pump. *Optics Express*, 22(S7):A1650–A1658, October 2014.

[24] D. J. Gray Jr., P. Santhanam, and R. J. Ram. Design for enhanced thermo-electric pumping in light emitting diodes. *Applied Physics Letters*, 103:123503–1–123503–5, September 2013.

[25] C. A. Wang, C. J. Vineis, H. K. Choi, M. K. Connors, R. K. Huang, L. R. Danielson, G. Nichols, G. W. Charache, D. Donetsky, S. Anikeev, and G. Belenky. Lattice-matched gainassb/algaassb/gasb materials for thermophotovoltaic devices. *AIP Conference Proceedings*, 653:324–334, 2003.

[26] Ioffe Physico-Technical Institute. Nsm archive - physical properties of semiconductors. http://www.ioffe.rssi.ru/SVA/NSM/Semicond/, January 2014. This database of material properties aggregates results from previously published materials.

[27] L. A. Coldren and S. W. Corzine. *Diode Lasers and Photonic Integrated Circuits*. Wiley-Interscience, 1995.

[28] M. Takeshima. Auger recombination in inas, gasb, inp, and gaas. *Journal of Applied Physics*, 43:4114–4119, October 1972.

[29] N. K. Dutta and R. J. Nelson. The case for auger recombination in $In_{1-x}Ga_xAs_yP_{1-y}$. *Journal of Applied Physics*, 53:74–92, January 1982.

[30] D. W. Winston. Simwindows32 version 1.5.0. Available online at http://ecee.colorado.edu/~ecen5355/f08/secure/simwindows.htm, May 2012. Copyright 1995 David W. Winston.

[31] D. J. Gray. Thermal pumping of light-emitting diodes. Master's of engineering, Massachusetts Institute of Technology, Department of Electrical Engineering and Computer Science, 2011.

[32] D. M. Rowe. *CRC Handbook of Thermoelectrics*. CRC-Press, 1995.

[33] J. B. Khurgin. Surface plasmon-assisted laser cooling of solids. *Physical Review Letters*, 98:177401–1–177401–4, April 2007.

[34] R. I. Epstein, M. I. Buchwald, B. C. Edwards, T. R. Gosnell, and C. E. Mungan. Observation of laser-induced fluorescent cooling of a solid. *Nature*, 377:500–503, October 1995.

[35] G. Y. Sotnikova, G. A. Gavrilov, S. E. Aleksandrov, A. A. Kapralov, S. A. Karandashev, B. A. Matveev, and M. A. Remennyy. Low voltage co_2-gas sensor based on iii-v mid-ir immersion lens diode optopairs: Where we are and how far we can go? *IEEE Sensors Journal*, 10(2):225–234, February 2010.

[36] D. Polder and M. Van Hove. Theory of radiative heat transfer between closely spaced bodies. *Physical Review B*, 4(10):3303–3314, November 1971.

[37] S. Shen, A. Narayanaswamy, and G. Chen. Surface phonon polaritons mediated energy transfer between nanoscale gaps. *Nano Letters*, 9(8):2909–2913, July 2009.